Apparent Slow Oceanic Transform Earthquakes Due to Source Mechanism Bias

Kimberly Schramm[1] and Seth Stein
Northwestern University

INTRODUCTION

Slow earthquakes, characterized as ones whose magnitude increases with period, are often observed occurring on oceanic transform faults (Kanamori and Stewart 1976; Okal and Stewart 1982; Stein and Pelayo 1991; Choy and Boatwright 1995; Newman and Okal 1998; Perez-Campos *et al.* 2003). Previous work has found that oceanic transform earthquakes often have lower body wave magnitudes compared to ridge and oceanic intraplate earthquakes of comparable surface wave magnitude and seismic moment. This phenomenon might result from the slow events having lower stress drop. Alternatively, the effect could be due to a source mechanism bias resulting from the fact that transform earthquakes are primarily strike-slip events on steeply dipping faults. In this geometry, body waves arriving at teleseismic distances left the source near nodal planes, resulting in smaller amplitudes than for dip-slip events of the same moment.

Slow earthquakes are ones that release energy more "slowly" than typical earthquakes and therefore radiate more energy at longer periods. Such earthquakes have been identified in various ways. One is from an anomalous ratio of the body wave magnitude m_b, which reflects the energy release at a period of 1 s, to the surface wave magnitude M_S, which reflects the energy release at a period of 20 s.

Although slow earthquakes have been observed in various tectonic environments, they are especially common for oceanic transform earthquakes that have strike-slip mechanisms, as shown by analysis of a global catalog of oceanic earthquakes (Stein and Pelayo 1991). The transform earthquakes generally had lower body wave magnitudes compared to ridge and oceanic intraplate earthquakes of comparable surface wave magnitude and seismic moment. This effect is illustrated in Figure 1A, where a transform event with a moment larger than the ridge event shown has lower m_b than the ridge event.

Other techniques have also been used to identify possible slow transform fault earthquakes. Some use the ratio of the energy in short-period body waves to the seismic moment to characterize the ratio of short- and long-period energy (Choy and Boatwright 1995; Newman and Okal 1998; Perez-Campos *et al.* 2003). Others use the shape of long-period source spectra to identify possible slow slip (McGuire *et al.* 1996; Abercrombie and Ekstrom 2003). These methods do not find "slowness" to be as pervasive as it appears from the magnitudes.

Slow earthquakes as defined by the magnitude differences can result from several effects (Stein and Wysession 2003). The most common is low stress drop, as illustrated in Figure 1B, which compares theoretical source spectra for earthquakes with the same seismic moment, M_0. The stress drop is a theoretical parameter proportional to the ratio of slip in the earthquake to its source dimension. For a given moment and fault shape, a lower stress drop corresponds to larger fault dimensions and therefore longer time functions and smaller corner frequencies. Thus, given two earthquakes with the same rupture velocity, the one with lower stress drop will have less high-frequency radiation and thus lower m_b. Hence the ratios of m_b/M_S and m_b/M_0 (or equivalently m_b/M_W where M_W is the moment magnitude) can be interpreted as indicating relative stress drops.

However, slow earthquakes need not reflect stress drop variations. One alternative is that similar effects can result from a slower rupture velocity, which also gives a longer time function for a given fault dimension. Another alternative is that differences in source mechanism can cause variations in m_b/M_S or m_b/M_0. This possibility is illustrated in Figure 1C, which shows focal mechanisms for a pure strike-slip event on a vertically dipping fault and a pure dip-slip event on a 45-degree dipping fault. Oceanic transform earthquakes are primarily strike-slip events on steeply dipping faults. As shown, body waves for such events that arrive at teleseismic distances left the source near nodal planes, resulting in smaller amplitudes than for dip-slip events of the same moment. A goal of this study is to assess whether this effect is large enough to produce the observed difference in magnitudes.

ANALYSIS AND MODELING

We explore two questions here. First, how convincingly do data show m_b/M_S or m_b/M_0 discrepancies between oceanic transform, ridge, and intraplate events? Second, if these differences are real, could they be due to the focal mechanism?

We began with the set of 142 earthquakes from 1964 to 1984 analyzed by Stein and Pelayo (1991). As shown in Figure 2A, the transform events generally have lower m_b for a given M_S or M_0 than the ridge and intraplate events. We then compiled a

1. Now at New Mexico Institute of Mining and Technology

doi: 10.1785/gssrl.80.1.102

(A) Seismograms from two events on a ridge-transform pair in the Gulf of California.

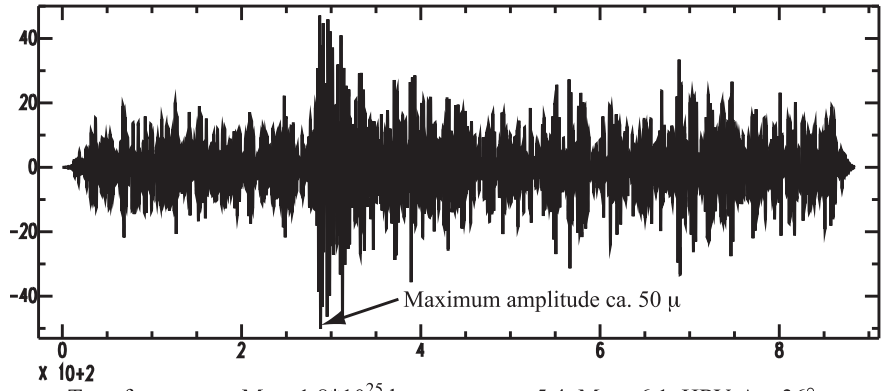

Transform event, $M_0 = 1.8*10^{25}$dyne-cm, $m_b = 5.4$, $M_w = 6.1$, HRV, $\Delta = 36°$

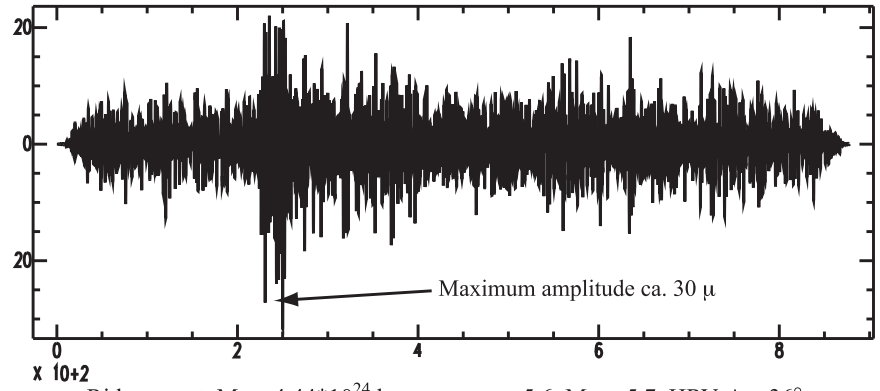

Ridge event, $M_0 = 4.44*10^{24}$dyne-cm, $m_b = 5.6$, $M_w = 5.7$, HRV, $\Delta = 36°$

(B) Effect of Stress Drop on moment and magnitude

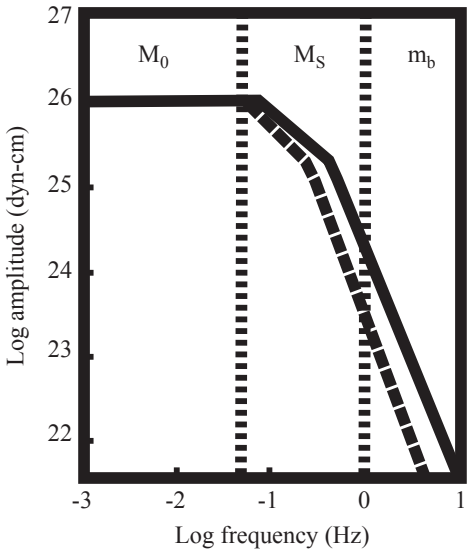

(C) Focal mechanisms commonly seen on mid-ocean ridges.

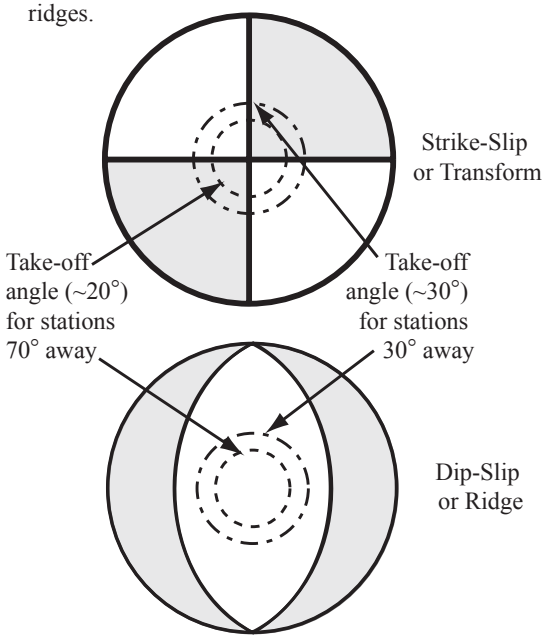

▲ **Figure 1.** (A) Seismograms from two events in the Gulf of California showing lower m_b for the transform event with higher M_0. (B) Schematic source spectra for low (dashed) and high (solid) stress drop events of the same moment. (C) Schematic illustration of a source mechanism bias on body wave amplitudes due to rays for strike slip events leaving the source closer to nodal planes.

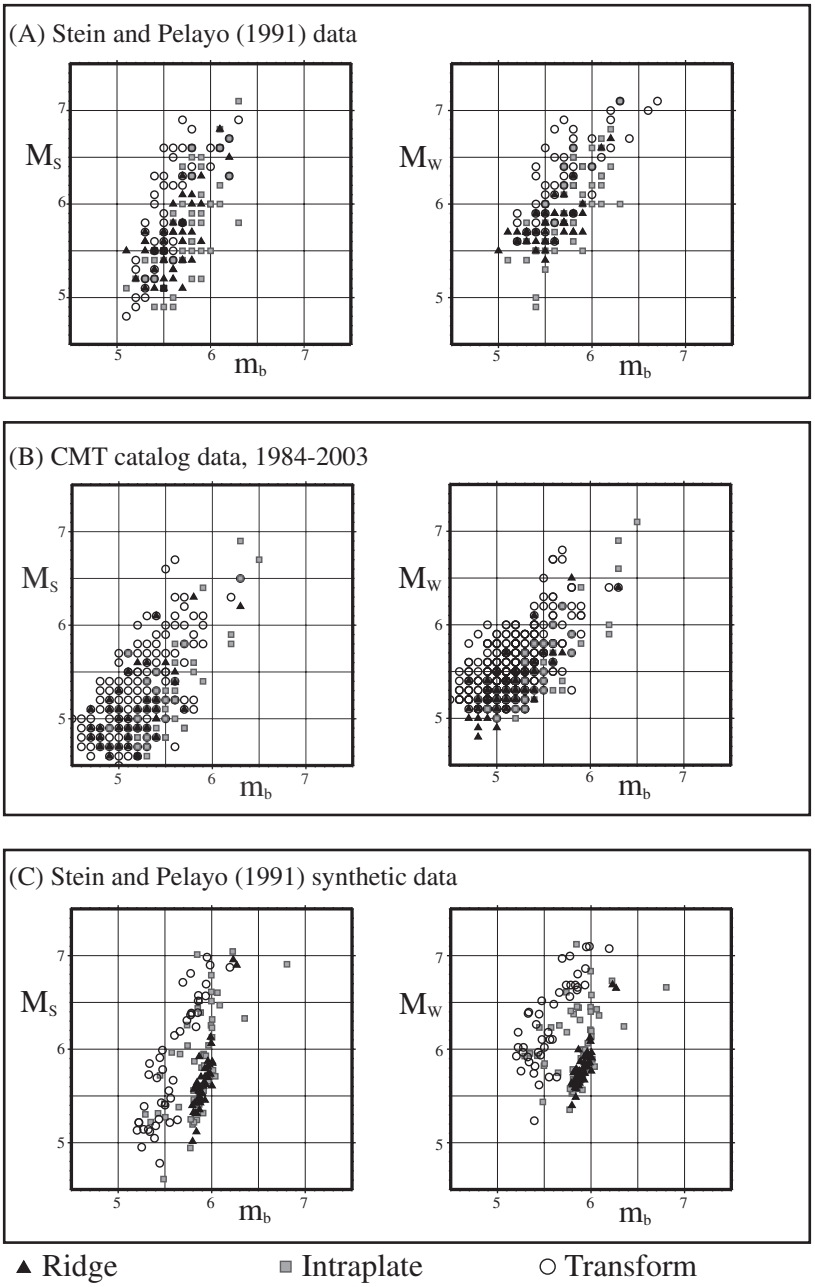

▲ **Figure 2.** Comparison of magnitudes observed for earthquakes (A and B) and measured on synthetic seismograms (C) for events with locations and mechanisms of those in (A). Circles that appear filled are overlapping events.

set of 419 additional events between 1984 and 2003 (Schramm 2007) with known focal mechanisms from the Harvard CMT catalog (now the Global CMT catalog). This larger dataset (Figure 2B) shows a similar pattern.

Given that the pattern is repeatable, we used body and surface wave modeling (Kanamori and Stewart 1976) to explore the possibility that it resulted from the differences in focal mechanisms rather than in stress drop. We generated synthetic seismograms for events with the locations, mechanisms, and moments of those in Figure 2A and measured body and surface wave magnitudes on the synthetic seismograms. This approach has the advantage that the differences in the measured magnitudes reflect only source mechanism differences, because other factors are held constant.

As shown in Figure 1B, the stress drop affects body and surface wave amplitudes via the source time function, which is the inverse Fourier transform of the source spectrum. Analytic expressions (Kanamori and Anderson 1975) are available that relate the stress drop to the seismic moment for several fault mechanisms and fault geometries. Following Geller (1976) we use the simplest, a circular fault model, to relate the stress drop

$$\Delta\sigma = (7/16)\, M_0 / R^3 \qquad (1)$$

to a source dimension or radius R for a given moment. We computed a fault source assuming a stress drop of 50 bars. In this approximation, the earthquakes under consideration have source dimensions of about 3–20 km. These are comparable to or longer than the wavelength of the body waves with period 1 s that are used to measure m_b. Hence the source dimension has a significant effect on body wave seismograms.

In the formulation we use, the source dimension controls the duration of the source time function, which can be described as a trapezoid resulting from the convolution of two "boxcar" functions. These have durations equal to the rupture time, T_R, reflecting the time needed for rupture to propagate along the fault and the rise time, T_D, over which slip occurs at any point. Assuming a circular fault, a shear velocity of 4 km/s and a rupture velocity (V_R) 0.7 times the shear velocity gives

$$T_R = R / V_R = 0.35R \text{ and } TD = 0.18R \quad (2)$$

(Geller 1976). Synthetic body wave seismograms were generated by scaling the source time function by the seismic moment and convolving it with a set of delta functions reflecting the source geometry and depth, and operators describing the effects of earth structure and a seismometer (Okal 1992).

We also generated synthetic surface wave seismograms, which did not require including the effect of source dimension. This is because the waves used to measure M_S (20-s period) and the longer period waves used to measure M_0 have wavelengths longer than the source dimension for the earthquakes in question. Hence although the source is finite for body waves, it is a point source for surface waves.

We calculated the magnitudes using the conventional formulas. Body wave magnitudes were derived from the largest amplitude measured at periods of 0.3–2.1 s on the short-period body wave synthetics using

$$m_b = \log (A/T) + Q(\Delta, h), \quad (3)$$

where A is the amplitude in microns of ground motion measured on the seismogram, T is the period in seconds, and the $Q(\Delta, h)$ values that vary with distance (Δ) and depth (h) are from the National Earthquake Information Center (NEIC), based on Gutenberg and Richter (1956). Surface wave magnitudes were calculated from synthetic seismograms for the vertical component of Rayleigh waves by measuring the largest amplitude between 18–22 s and using the International Association of Seismology and Physics of the Earth's Interior (IASPEI) formula

$$M_s = \log (A/T) + 1.66 \log \Delta + 3.3 \quad (4)$$

For each earthquake in Figure 2A we synthesized seismograms at 10 stations with varying azimuths and distances. The magnitudes were measured for each station and their average is shown in Figure 2C.

The stations were picked by looking up each event in the ISC catalog and downloading the list of stations reporting arrivals. A computer program read in the list and found one station for each of 10 azimuthal bins between 0–360 degrees. Events without good azimuthal coverage were discarded. Distances for the stations varied from 30 to 70 degrees.

Examination of the magnitudes derived from the synthetic seismograms shows two gratifying features. First, the general range and trend of the body and surface magnitudes from the synthetic seismograms are similar to those in the two datasets. Hence it appears that the earthquake source and earth model parameters used to generate the synthetics are reasonable. Second, the variation in body and surface magnitudes between transform and other events in the synthetic seismograms are similar to those in the data. It seems likely that the observed variation is due largely to the differences in focal mechanism.

DISCUSSION

Our modeling shows that for earthquakes with the same seismic moment and source time function duration, strike-slip events will appear slow relative to dip-slip events because of their lower body wave amplitudes. This slowness is apparent in that because it reflects the effects of the radiation pattern rather than the source spectrum. It arises because magnitudes are measured directly from seismograms and not corrected for the source radiation pattern.

Although this procedure identifies slow earthquakes by comparing two measured magnitudes, the magnitudes do not directly yield an estimate of stress drop. Estimation of the stress drop from observations first requires estimating the source dimension or dimensions directly or indirectly from either source spectra in the frequency domain or the source time function. This requires assumptions about the rupture velocity, rise time, and fault geometry, including whether rupture propagation was unilateral or bilateral. Often only one dimension is estimated from the data, and the other is inferred for the assumed fault geometry. Because the inferred stress drop depends on the inverse cube of the estimated source dimension, small changes in the estimated dimensions have large effects on the estimated stress drop (Chung 1979; Stein and Kroeger 1980).

Additional uncertainties result because further assumptions are needed to infer stress drop from the estimated source dimensions, as illustrated in Table 1 and Figure 3. Depending on these assumptions, quite different stress drop values would be inferred. As shown in Table 1's first row, the stress drop for a given seismic moment depends on the focal mechanism (columns) and fault geometry (R or L and w) (Kanamori and Anderson 1975, their Figure 1). The second row shows how estimates of the stress drop can vary for different geometries with the same seismic moment and source dimension (L or R). For example, compared to the stress drop inferred for a circular fault, assuming slip on a square rupture (shape factor $C = L/w = 1$) with strike-slip or dip-slip motion yields stress drops about 50% or 100% larger (Figure 3). The inferred stress drop is even greater for narrower (greater C) ruptures. Similar issues arise in estimating the stress drop for events with the same

TABLE 1
Relations Between Stress Drop, Fault Geometry, and Fault Dimension

	Circular	Strike Slip	Dip Slip
$\Delta\sigma$	$\frac{7}{16}\frac{M_0}{R^3}$	$\frac{2}{\pi}\frac{M_0}{w^2 L}$	$\frac{8}{3\pi}\frac{M_0}{w^2 L}$
$\Delta\sigma$	$\frac{7}{16}\frac{M_0}{R^3}$	$\frac{2C^2}{\pi}\frac{M_0}{L^3}$	$\frac{8C^2}{3\pi}\frac{M_0}{L^3}$
S	πR^2	$\frac{L^2}{C}$	$\frac{L^2}{C}$
$\Delta\sigma$	$\frac{7\pi^{3/2}}{16}\frac{M_0}{S^{3/2}}$	$\frac{2C^{1/2}}{\pi}\frac{M_0}{S^{3/2}}$	$\frac{8C^{1/2}}{3\pi}\frac{M_0}{S^{3/2}}$

w = fault width, L = fault length, $C = L/W$, S = fault area.

seismic moment and fault area, and thus slip, as shown in Table 1, fourth row, and the right-hand side of Figure 3.

Thus although the transform earthquakes appear slow in that they have relatively less short-period energy on seismograms at teleseismic distances, there is no clear case for assuming that they have lower stress drop. We have shown that the observed differences in magnitudes would occur between strike-slip and dip-slip earthquakes of the same moment and source time function duration. As Table 1 shows, such earthquakes would have the same stress drop using a circular rupture model. However, they would have different stress drops in the rectangular fault models. The larger transform events would likely occur on longer and narrower faults than the dip-slip ridge and intraplate events. This geometry may explain the observation that the transform events have lower ratios of seismic moment to time function duration cubed than ridge and intraplate events (Stein and Pelayo 1991). Although this observation would be consistent with transform events having low stress drop, it would also be consistent with the transform events having the same stress drop but on longer and narrower faults. Resolving these issues for earthquakes observed at teleseismic distances like those discussed here will be difficult except for the largest earthquakes, where seismological data provide more information about the fault geometry.

These results bring out the recognized issue that although "stress drop" can be inferred from seismograms, albeit with large uncertainties, this seismologically estimated parameter may—or may not—reflect the stress change during rupture (Atkinson and Beresnev 1997). Moreover, what if any relation it has to the state of stress on the fault is unclear (Kanamori 1977). The idea

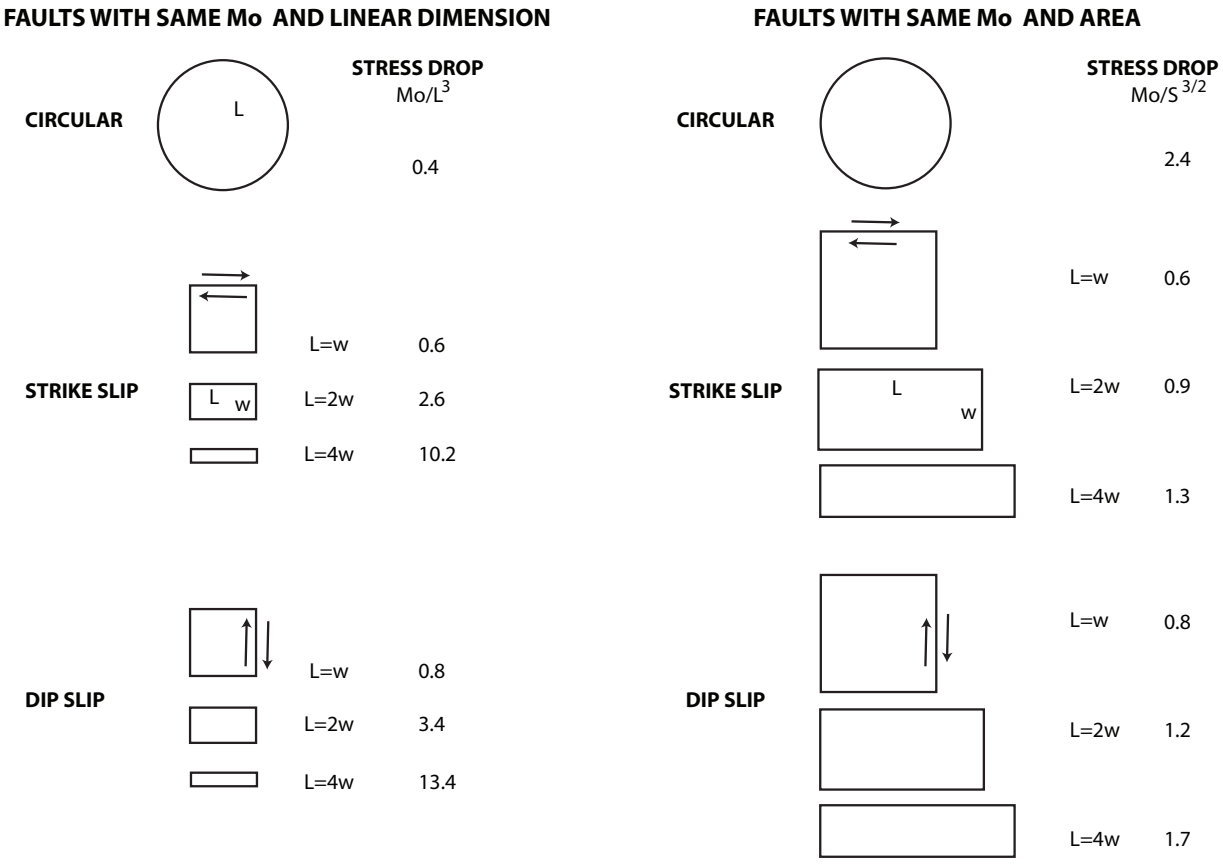

▲ **Figure 3.** Left side: comparison of stress drop for faults with the same moment and source dimension, but different focal mechanism and fault geometry. Right side: comparison of stress drop for faults with the same moment and source area, but different focal mechanism and fault geometry.

of slow events being due to low stress drop is intuitively appealing, as is the idea that active transforms may be weaker than other oceanic crust. However, the results here imply that the apparent slowness of transform events implied by their magnitudes is largely due to their strike-slip mechanisms. This result would partly explain why other techniques for identifying slow earthquakes, which are either less affected by this bias or correct for it, find fewer slow events on oceanic transforms.

ACKNOWLEDGMENTS

We thank Emile Okal for insightful discussions.

REFERENCES

Abercrombie, R. E., and G. Ekstrom (2003). A reassessment of the rupture characteristics of oceanic transform earthquakes. *Journal of Geophysical Research* **108**; doi:10.1029/2001JB000814.

Atkinson, G. M., and I. Beresnev (1997). Don't call it stress drop. *Seismological Research Letters* **368**, 3–4.

Choy, G. L., and J. Boatwright (1995). Global patterns of radiated seismic energy and apparent stress. *Journal of Geophysical Research* **100**; doi:10.1029/95JB001969.

Chung, W. -Y. (1979). Variation of seismic source parameters and stress drop within a descending slab as revealed from body wave pulse width and amplitude analysis. PhD dissertation part I, California Institute of Technology, Pasadena, CA.

Geller, R. J. (1976). Scaling relations for earthquake source parameters and magnitudes. *Bulletin of the Seismological Society of America* **66**, 1,501–1,523.

Gutenberg, B. and C. F. Richter (1956). Magnitude and energy of earthquakes. *Annali di Geofisica* **9**, 1–15.

Kanamori, H. (1977). The energy release in great earthquakes. *Journal of Geophysical Research* **82,** 2,981–2,987.

Kanamori, H. and D. L. Anderson (1975). Theoretical basis of some empirical relations in seismology. *Bulletin of the Seismological Society of America* **65**, 1,073–1,095.

Kanamori, H., and G. S. Stewart (1976). Mode of the strain release along the Gibbs fracture zone, Mid-Atlantic Ridge. *Physics of the Earth and Planetary Interiors* **11**, 312–332.

McGuire, J. J., P. F. Ihmle, and T. H. Jordan (1996). Time-domain observations of a slow precursor to the 1994 Romanche transform earthquake. *Science* **274**, 82–85.

Newman, A. V., and E. A. Okal (1998). Teleseismic estimates of radiated seismic energy: The E/M_0 discriminant for tsunami earthquakes. *Journal of Geophysical Research* **103**; doi 10.1029/98JB02236.

Okal, E. A. (1992). A student's guide to teleseismic body wave amplitudes. *Seismological Research Letters* **63**, 169–180.

Okal, E. A., and L. M. Stewart (1982). Slow earthquakes along oceanic fracture zones: Evidence for asthenospheric flow away from hot spots. *Earth and Planetary Science Letters* **57**, 75–87.

Perez-Campos, X., J. J. McGuire, and G. C. Beroza (2003). Resolution of the slow earthquake/high apparent stress paradox for oceanic transform fault earthquakes. *Journal of Geophysical Research* **108**; doi:10.1029/2002JB002312.

Schramm, K. A. (2007). The role of source mechanism geometry in biasing estimates of earthquake slowness. PhD dissertation, Northwestern University, Evanston, IL, 94 pps.

Stein, S., and G. C. Kroeger (1980). Estimating earthquake source parameters from seismological data. In *Solid Earth Geophysics and Geotechnology*, ed. S. Nemat-Nasser, 61–71. New York: American Society of Mechanical Engineers.

Stein, S., and A. Pelayo (1991). Seismological constraints on stress in the oceanic lithosphere. *Philosophical Transactions of the Royal Society of London*, Series A, **337**, 53–72.

Stein, S., and M. Wysession (2003). *An Introduction to Seismology, Earthquakes, and Earth Structure*. Malden, MA: Blackwell Publishing, 498 pps.

Department of Earth and Environmental Science
New Mexico Institute of Mining and Technology
Socorro, New Mexico 87801 U.S.A.
schramm@ees.nmt.edu
(K. S.)